J. Fluid Mech. (1995), *vol.* 301, *pp.* 203-223

A numerical study of pulsating flow behind a constriction

By MOSHE ROSENFELD

Department of Fluid Mechanics and Heat Transfer, Faculty of Engineering,
Tel Aviv University, Tel Aviv 69978, Israel

(Received 11 May 1993 and in revised form 31 May 1995)

The flow field behind a constricted channel is studied numerically. A pulsating incoming flow with a non-vanishing mean is imposed at the entrance and the flow field is investigated for a wide range of Reynolds and Strouhal numbers ($1500 > Re > 45$, $12 > St > 0.01$). In most cases (except at the two ends of the Strouhal number regime or for $Re < 90$), propagating vortices are found downstream of the constriction with a wavy core flow between them. The size and number of coexisting vortices depend on St but less on Re. The strength and structure of the vortical regions depend on both Re and St. The formation of the vortices is discussed for the various St regimes and the characteristics of the vortical flow are described.

1. Introduction

The study of pulsating flows in channels has received increased attention in the past few years both in engineering and biofluid applications, e.g. Sobey (1982, 1985), Armaly *et al.* (1983), Pedley & Stephanoff (1985), Ralph (1986), Ralph & Pedley (1988, 1989), Park (1989), Tutty (1992) and Tutty & Pedley (1993, 1994). Unsteady flows in general, and pulsating flows in particular, exhibit an exceptionally large variety of flow structures that strongly depend on the governing parameters, such as the Reynolds and Strouhal numbers. Of special interest are the vortical structures that were found to develop in non-uniform channels. The swirling motion of the vortices significantly alters the characteristics of derived quantities, such as heat transfer and mixing rates. Thus, the identification of possible flow structures in pulsating flows and their dependence on the governing parameters is of importance to fundamental and applied research.

In the present study, we focus on incompressible viscous flows in two-dimensional constricted channels. Even cases with steady entrance flow may exhibit complex flow patterns, Armaly *et al.* (1983). Depending on the geometry and flow conditions, several separation eddies may be generated behind the constriction, and at Reynolds numbers of $O(10^3)$, the flow becomes unsteady and vortices are shed periodically. Moving vortices are found at substantially lower Reynolds numbers ($O(10^2)$), if a pulsating flow is imposed by an oscillating indentation (Pedley & Stephanoff 1985; Ralph & Pedley 1988, 1989) or by pulsating or oscillating incoming flow (Sobey 1985; Park 1989; Tutty 1992; Tutty & Pedley 1993). The moving vortices at low Reynolds numbers owe their existence to stable flow processes, in contrast to vortex shedding that acts at considerably higher Reynolds numbers. A summary of several relevant studies is given in table 1, where Re and St refer to the Reynolds and Strouhal numbers, respectively.

Authors	Geometry	Oncoming flow	*Re*	*St*	Main findings
Pedley & Stephanoff (1985). Experimental.	Oscillating indentation	Steady	$1260 > Re > 360$	$0.077 > St > 0.0052$	Vortex waves generated by inviscid mechanism. Induce eddies that may double.
Ralph & Pedley (1988, 1989). Numerical.	Oscillating indentation	Steady	507, 600, 670	0.019, 0.037, 0.057	Verified experimental results of Pedley & Stephanoff. Vortex waves were found in all cases. Identified viscid and inviscid contributions.
Sobey (1985). Experimental & numerical.	Asymmetric & symmetric	Steady or oscillating	$500 > Re > 5$	$0.24 > St > 0.0012$	Asymmetric channels: vortex waves, stationary vortices. Symmetric channels: vortex shedding, moving vortices. Flow is not sensitive to the shape of the constriction (for similar size).
Ralph (1986). Numerical & experimental.	Sinusoidal (rigid) walls, symmetric	Oscillating	$300 > Re > 50$	$0.08 > St > 0.005$	Time asymmetry for high *St*. Types of flows were mapped in the (*Re*, *St*) plane.
Tutty (1992). Numerical.	Half-circular constriction	Sinusoidal +mean, physiological	500, 750	0.024, 0.048	Strong vortex waves even for small *St*, increases in strength with *St* and *Re*. Wavelength independent of *Re*, inversely proportional to *St*. Wall shear significantly larger than in steady flow.
Tutty & Pedley (1993). Numerical.	Stepped channel	Oscillating	250, 500, 750	0.004, 0.006, 0.010	Strong vortex wave during the forward phase. Secondary effects result in complex flow patterns. Eddies with more than one core.
Park (1989). Experimental.	Circular-arc constriction	Pulsating (2.3)	$350 > Re > 120$†	$0.55 > St > 0.19$†	Two trains of propagating vortices.

† Based on the mean velocity

TABLE 1. Summary of existing works

The experiments of Pedley & Stephanoff (1985) found a wavy core flow with two trains of downstream propagating eddies behind an oscillating indentation. They showed analytically that the wave generation process is essentially inviscid, but certain processes related to the eddies (such as eddy doubling) are inherently viscid. Ralph & Pedley (1988, 1989) simulated numerically the experiments of Pedley & Stephanoff (1989) and obtained good agreement. Their work also clarified the role of viscosity in the development of eddies.

Another way of obtaining pulsating flows is by enforcing an oscillating incoming flow in a channel with rigid walls. Sobey (1982) and Ralph (1986) considered channels with sinusoidal walls. Channels with a single constriction were studied by Sobey (1985), Park (1989), Tutty (1992) and Tutty & Pedley (1993). Sobey (1985) and Tutty & Pedley (1993) studied oscillating incoming flows with a zero mean, while Park (1989) and Tutty (1992) considered pulsating flows with a non-vanishing mean. Although the geometry and the incoming waveform were different in each case, vorticity waves were found in all the cases with eddies beneath the crests and above the troughs of the wavy core flow. Sobey (1985), Tutty (1992) and Tutty & Pedley (1993) found essentially stationary vortices, while Pedley & Stephanoff (1985), Ralph & Pedley (1988, 1989) and Park (1989) observed downstream propagating vortices.

Probably the single most distinctive property of periodically forced flows is their strong dependence on the governing non-dimensional numbers, such as the Strouhal or Reynolds numbers. Table 1 shows that existing works studied laminar flows at intermediate Re and usually low St. Even at this narrow range, variations in the flow details could be identified. The incoming waveform and the shape of the constriction seem to have a less important effect on the global properties of the flow field.

The aim of the present work is to study further vortex generation and propagation in pulsating flows behind constricted channels by extending the governing parameter regimes. The sensitivity of the flow to numerous variables does not allow a single study to be carried out that covers the entire parameter regime. Therefore, the study focuses on two of the most important factors: the Strouhal and Reynolds numbers. The Strouhal number is varied by three orders of magnitudes ($12 > St > 0.01$), while the Reynolds number is changed by almost two orders of magnitude ($1500 > Re > 45$).

The study is based on the solution of the Navier-Stokes equations using an existing, well-validated numerical method, see Rosenfeld, Kwak & Vinokur (1991) and Rosenfeld & Kwak (1991, 1993). The geometry of the constriction and the incoming waveform were chosen to be similar to the experimental set-up of Park (1989), to permit the validation of the numerical model. The details of the validation procedure are given in Rosenfeld (1993). The present work relies on the good agreement obtained to extend the parameter range and to study the flow in a detail not possible using experimental techniques only.

The formulation of the problem and the numerical model are briefly described in §2. In the presentation of the results, first the flow details for a base case are given in §3 along with a discussion on the formation of the vortical flow field. The dependence on Re is discussed in §4 for a given St, while the effect of St is discussed in §5 for a fixed Re. In §6, primary and secondary flow processes that affect the vortical flow behind the constriction are discussed.

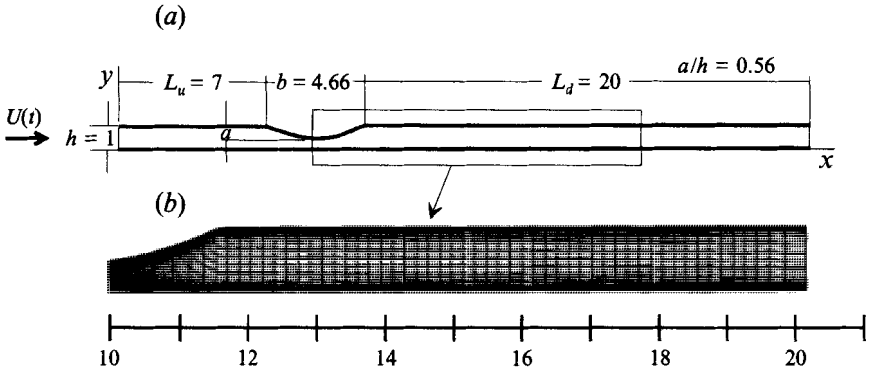

FIGURE 1. (*a*) The geometry of the computational domain (not to scale) and (*b*) the mesh in the region downstream of the constriction (only every fourth mesh point is shown).

2. Formulation and numerical model

2.1. *Geometry and mesh*

The geometry of the computational domain is sketched in figure 1(*a*). The channel is composed of two straight parallel plates at a distance of h from each other (all length units are scaled by h). On the upper wall, a circular-arc constriction is added with a size of $a/h = 0.56$ (other constriction sizes were checked as well, but this one produced the more interesting and manageable flow simulations). The upstream and downstream boundaries are at a distance of $L_u = 7$ and $L_d = 20$ from the respective edges of the constriction. A mesh with 97×417 points in the transverse and axial directions, respectively, is generated by a transfinite algebraic mesh generator. A blow-up of the grid in the region downstream of the constriction is shown in figure 1(*b*); for clarity, only every fourth point is shown in each direction.

2.2. *Governing equations and boundary conditions*

The equations governing the flow of a constant-density isothermal incompressible fluid in a fixed control volume with face S and volume V are the conservation of mass

$$\oint_S \mathrm{d}\boldsymbol{S}\cdot\boldsymbol{u} = 0 \tag{2.1}$$

and the Navier–Stokes equations

$$\frac{\mathrm{d}}{\mathrm{d}t}\int_V \boldsymbol{u}\,\mathrm{d}V = \oint_S \mathrm{d}\boldsymbol{S}\cdot\boldsymbol{T}, \tag{2.2a}$$

where $\boldsymbol{u}$ is the velocity vector, t is the time, $\mathrm{d}V$ is a volume element and $\mathrm{d}\boldsymbol{S}$ is the area element vector. For Newtonian fluids the tensor $\boldsymbol{T}$ is given by

$$\boldsymbol{T} = -\boldsymbol{u}\,\boldsymbol{u} - P\boldsymbol{I} + \nu\left(\nabla\boldsymbol{u} + (\nabla\boldsymbol{u})^T\right), \tag{2.2b}$$

where $\boldsymbol{I}$ is the identity tensor, $\nabla\boldsymbol{u}$ is the gradient of $\boldsymbol{u}$ and $(\nabla\boldsymbol{u})^T$ is its transpose. The pressure is P and ν is the kinematic viscosity.

The incoming axial velocity (or mass flow rate), $U(t)$, is forced to:

$$\left.\begin{aligned} U(t) &= U_s, && 0 < t/T \leqslant 1/2, \\ U(t) &= U_s - U_p \sin(2\pi t/T), && 1/2 < t/T \leqslant 1, \end{aligned}\right\} \tag{2.3}$$

i.e. a half-sine is superimposed on the steady flow during the second half of the cycle. The period is T and U_s, U_p are the steady and oscillating components, respectively. The geometry of the constriction and the incoming waveform are similar to that used by Park (1989) in his series of flow visualizations. The start of each cycle is at $t/T = 0$ and t/T is the phase of the cycle. We shall also refer to a phase in the cycle according to the variation of the incoming flow. Thus, the steady incoming flow phase refers to the first half of the cycle, $1/2 > t/T \geqslant 0$, while the acceleration and deceleration phases refer to $3/4 > t/T \geqslant 1/2$ and $1 > t/T > 3/4$, respectively.

At the upstream boundary, a fully developed flow between two straight plates is specified for the waveform given by (2.3). At the downstream boundary, Neumann-type conditions are given for the velocity components: $\partial \boldsymbol{u}/\partial x = 0$, where x is the streamwise Cartesian coordinate. On the upper and lower solid walls, the no-slip and no-injection conditions are specified, $\boldsymbol{u} = 0$.

2.3. *The numerical scheme*

The laminar unsteady incompressible Navier–Stokes equations with primitive variables are solved with a solution procedure developed by Rosenfeld *et al.* (1991) and Rosenfeld and Kwak (1991, 1993). The formulation of the governing equations, the discretization procedure and the numerical solution stages are combined to yield an accurate and efficient solution method of complex time-dependent flows in generalized coordinate systems. The governing equations, written in the integral form (2.1) and (2.2), are discretized by finite volumes. The Cartesian velocity components are replaced by the volume fluxes across the faces of the computational cells as the dependent variables, in addition to the pressure. The scheme is second-order accurate in space and time. The discrete equations are solved by a fractional step method with an approximate factorization of the momentum equations. The convergence rate of the Poisson equation is accelerated by a multigrid procedure. The interested reader may find the details of the method in the references cited above.

2.4. *Description of the cases*

In the present work, the effects of the constriction size and waveform will not be considered. Under these conditions two non-dimensional parameters, the Reynolds $Re = U_m h/\nu$ and Strouhal $St = h/U_m T$ numbers govern the flow field (U_m is the mean velocity). The non-dimensional velocity components of the waveform were set to $U_s = 1$ and $U_p = 1.22$, yielding a mean velocity of $U_m = 1.39$.

A base case, which resulted an interesting and representative flow field, was chosen with $Re = 360$ and $St = 0.368$. The variations in St and Re are made independently about the base case. The parameters of the base case are close to a case previously validated against the experimental results of Park (1989), see Rosenfeld (1993). A relatively wide range of St and Re were simulated in the present study. The Reynolds numbers solved for $St = 0.368$ were $Re = 45$, 90, 180, 360, 720 and 1440, while for $Re = 360$ the following Strouhal numbers were solved: $St = 0$ (steady incoming flow), 0.011, 0.023, 0.046, 0.092, 0.184, 0.368, 0.491, 0.737, 0.982, 1.310, 1.473 and 11.787.

2.5. *Numerical details and accuracy*

The solution was started from a fully developed parabolic velocity profile and was marched in time until a time-periodic flow was attained in the whole region of interest. The number of cycles needed to establish a time-periodic solution depends mainly on the Strouhal number, because convection is the main mechanism of propagating the disturbances. For the base case 20 cycles were needed, while for $St = 0.011$ and

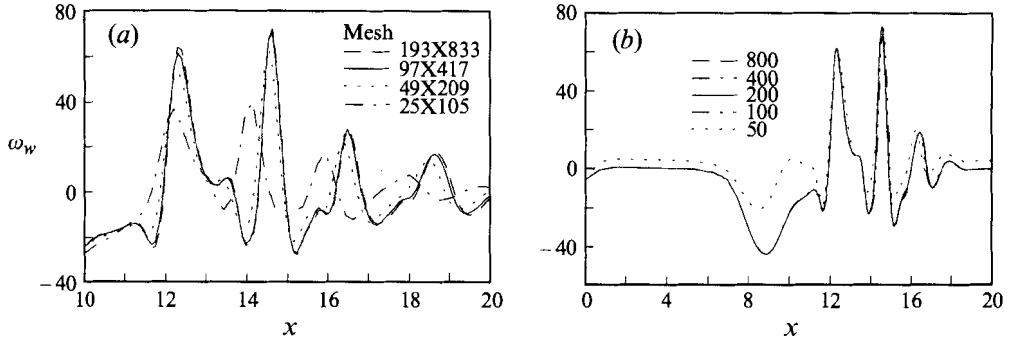

FIGURE 2. (*a*) Mesh and (*b*) time-step refinement studies of the lower-wall vorticity.

11.787, 3 and 400 cycles were calculated, respectively, until a graphically accurate periodic flow was established. All the results to be presented are for the periodic flow. Thus, $t/T = 0.1$ and $t/T = 1.1$ refer to the same phase of the cycle and $t/T = 0$ refers to the start of the cycle and not to the start of the calculations.

The numerical method has been validated for a series of internal and external flow problems, e.g. Rosenfeld *et al.* (1991) and Rosenfeld & Kwak (1991). The numerical model of the channel was validated in a previous paper, Rosenfeld (1993). Very good agreement was obtained with the experimental results of Park (1989) for a different set of parameters.

Additional mesh and time-step refinement studies were carried out in the present study for the base case. The wall vorticity was found to be a sensitive quantity for performing the tests. Figure 2(*a*) summarizes a mesh refinement study on the lower-wall vorticity for $t/T = 0.2$. Four meshes with 25×105, 49×209, 97×417 and 193×833 points were employed; ten cycles with 200 time steps per cycle were calculated in all the cases. The solution shows sensitivity to the mesh size, but the grid of 97×417 points seems to result in a good compromise between accuracy and efficiency. It should be noted that other flow variables are less mesh dependent and an accurate solution away from the walls is obtained for even coarser meshes. Nevertheless, in the present study we used the mesh of 97×417 points in all the calculations.

A time-step refinement study for the mesh of 97×417 points is given in figure 2(*b*) for $t/T = 0.2$. The solution shows time-step independence for $N_c > 100$, where N_c is the number of time steps per cycle. Therefore, 200 time steps were employed for the base case. For other periods, the number of time steps was changed proportionally, but it was never less than $N_c = 100$, even for the largest Strouhal number.

In addition, the placement of the upstream and downstream boundaries and the type of boundary conditions were tested. The conditions given in §2.1 and §2.2 reflect the values that were found not to affect the solution in the regions of interest.

3. The base case ($Re = 360$, $St = 0.368$)

3.1. *Steady flow*

A case with a steady incoming flow ($St = 0$), referred to as the equivalent steady flow, was first solved. A parabolic velocity profile was specified on the upstream boundary with a mass rate flow equal to the mean of the pulsating case ($U(t) = U_m = 1.39$). The streamlines are shown in figure 3; a steady flow is obtained with an elongated stationary eddy in the lee of the constriction. In the downstream part of the eddy, the

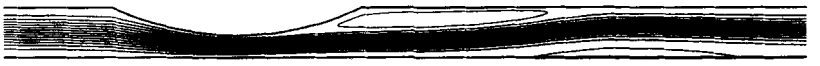

FIGURE 3. The streamlines of the equivalent steady flow ($Re = 360$, $St = 0$). Flow is from left to right.

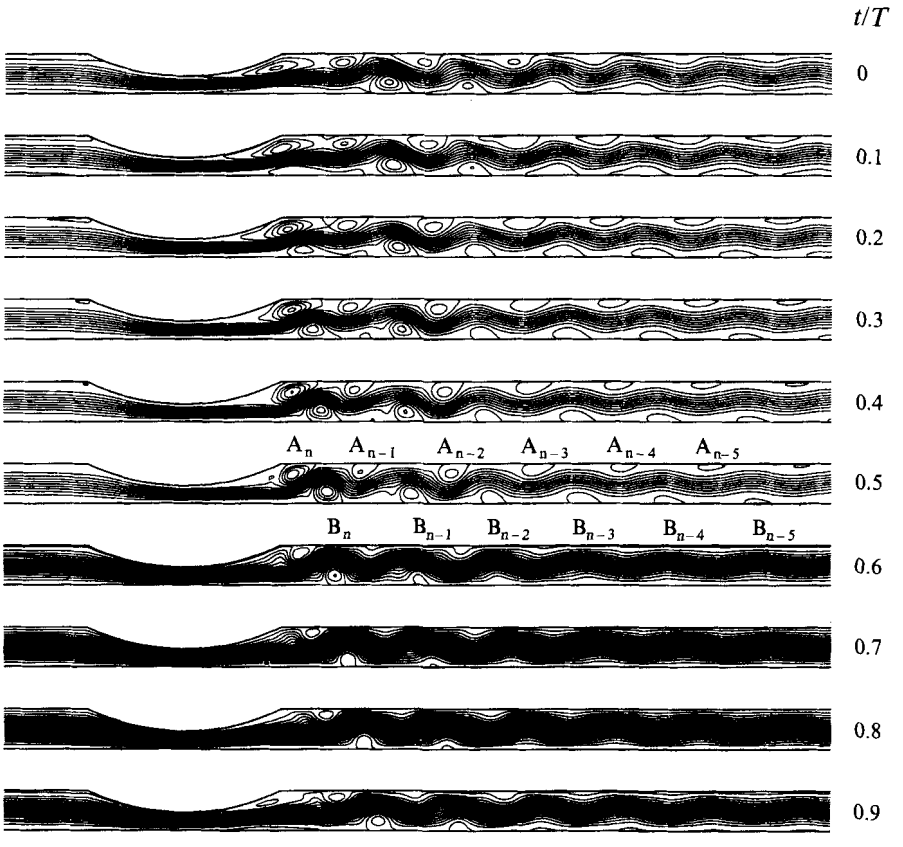

FIGURE 4. The instantaneous streamlines at 10 equally spaced instants of a cycle ($Re = 360$, $St = 0.368$).

core flow streamlines have an upward slope, inducing the creation of a smaller eddy on the lower wall as well. At a distance of about 10 channel height units downstream of the constriction, the flow returns to be fully developed.

3.2. *Description of the flow*

The instantaneous streamlines of the base case ($Re = 360$, $St = 0.368$) are shown in figure 4 for 10 equally spaced instants along one cycle. In the first half of the cycle, a vortex is observed on the upper wall in the lee of the constriction, followed by a series of decaying vortices downstream. On the lower wall, another series of vortices is observed. The vortices propagate downstream, resulting in a wavy core flow with decreasing lateral oscillations in the downstream direction. In the acceleration phase of the cycle ($3/4 > t/T > 1/2$), the vortices seem to diminish rapidly, the streamlines straighten out and the flow in the diverging part of the constriction attaches to the walls. In the deceleration phase ($1 > t/T > 3/4$), the vortex in the lee of the constriction reappears, along with the other vortices in the field that seemed

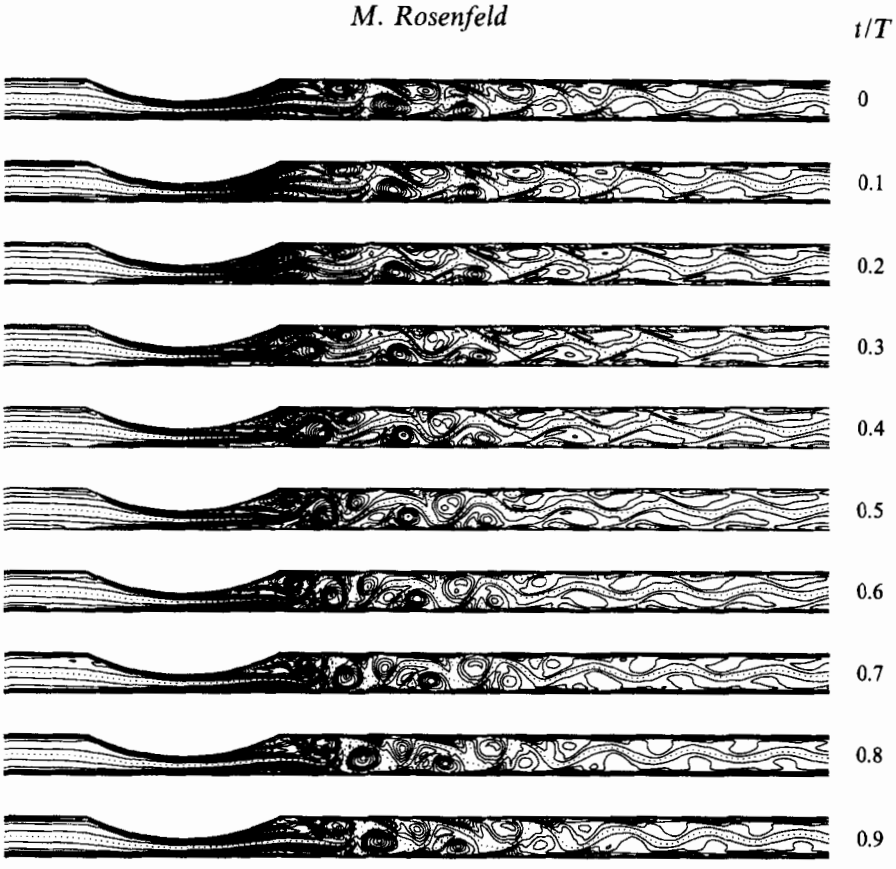

FIGURE 5. The vorticity field at 10 equally spaced instants of a cycle ($Re = 360$, $St = 0.368$). The increment between the contour lines is 2.5. Zero values are shown by dotted lines.

to disappear during the acceleration phase. In the steady phase of the incoming flow, the vortices expand and get stronger.

The pattern of the streamlines is very useful in analysing steady flows, yet it might be misleading in the case of forced unsteady flows with large amplitudes of the oscillating components. The large increase in the incoming velocity wrongly implied the disappearance of the vortices in the plots of the instantaneous streamlines, as figure 5 clearly exhibits. In this figure, the vorticity contour lines are given for the same 10 equally spaced time intervals. The transverse oscillations in the vorticity field remain fairly uniform over the whole cycle, in contrast to what was observed in the pattern of the streamlines. The difference is especially visible in the acceleration phase of the flow, when the instantaneous streamlines are almost parallel to the walls, while the vorticity field still exhibits large lateral variations. The streamlines also indicated the diminishing of the vortices in the acceleration phase and their reappearance in the deceleration phase. The vorticity field, however, reveals that the size and the strength of the vortices† hardly change.

Figures 4 and 5 show that a new pair of vortices is developed in each cycle, one vortex near each wall. At any instant, vortices generated in previous cycles still coexist downstream, creating the two trains of moving vortices near the walls and the

† Following the roll-up of the vortices (see §3.3), they can be identified by the closed, almost circular vorticity contour lines. The size and strength of the vortices correlate with the extent and magnitude of the closed vorticity contour lines.

wavy core flow between them. Following the notation of Park (1989), the upper- and lower-wall vortices are labelled by A and B, respectively (figure 4). The coexisting vortices are distinguished by an index that refers to the formation cycle relative to the present cycle n. Thus, B_{n-1} refers to the lower-wall vortex that was generated in the previous cycle, etc.

The pulsating incoming flow leads to a very different flow than the equivalent steady flow, although the mean incoming velocity is equal. In the pulsating case, two trains of moving vortices are generated, while in the steady case two stationary eddies grow next to the constriction, one near each wall. Moreover, the vortices of the pulsating case are small in length and nearly circular in shape, while in the steady case the eddies have an elongated shape with a relatively small height. Obviously, the differences should be attributed to the pulsating nature of the incoming flow.

The flow field of the base case raises several issues; some of them are listed below. What is the formation mechanism of the vortical flow field? Are the vortices created as a response to the core flow or vice versa? What are the roles of the forced pulsating flow and the geometric non-uniformity in the development of the vortical flow? How do the Reynolds or Strouhal numbers affect the flow field? These and other issues will be addressed in the rest of the paper.

3.3. *Formation of vortices*

The generation of pairs of vortices in each cycle and their propagation downstream was also observed experimentally by Park (1989) for a lower Reynolds number. He described the gross features of the flow based on the visualizations of the instantaneous streamlines. Yet, Park (1989) neither discussed the fine details of the flow field nor the formation mechanism of the vortices, probably because the resolution of the experimental visualizations was inadequate. Our high-resolution calculations do allow a detailed discussion of the vortex formation mechanism for the base case. The formation of the vortices in other regimes of the Strouhal number is discussed in §6.1.

The formation region of the first pair of vortices (A_n and B_n) ranges from $x \approx 11$ to $x \approx 13$, figures 4 and 5. The events that lead to the growing of a pair of vortices in each cycle are further depicted in figure 6, where the streaklines are shown for the deceleration and part of the steady incoming flow phases (note that because of the periodicity, $t/T = 0.2$ and 1.2, for example, refer to the same phase of the cycle). The first instant shown is $t/T = 0.8$, that is at the start of the deceleration phase. The vortices generated in the previous cycle (A_{n-1} and B_{n-1}) can still be observed downstream. In the expanding part of the constriction (except near the downstream end), the streaklines are parallel to the walls. In the middle of the deceleration phase ($t/T = 0.9$), the increase in the lateral velocity (as was determined from the sequence of lateral velocity plots) displaces the streaklines away from both walls. At the end of the deceleration phase ($t/T = 1$) the streaklines, which represent shear layers (figure 5), penetrate rapidly into the core. A large region of separated flow is formed in the lee of the constriction, but no roll-up is yet evident. These processes further intensify at the beginning of the steady phase and the outer parts of the streaklines reach the core flow ($t/T = 1.1$). The downstream parts of the streaklines turn back owing to the initiating of the roll-up process and by $t/T = 1.3$, A_n and B_n are fully formed.

The roll-up of A_n starts and completes earlier than for B_n. Yet, the difference in the roll up time is small (less than 0.05 of the period). The vortex B_n is formed in response to the formation of A_n (see §6.1). The shear layers that create A_n and B_n originate from the throat of the constriction (see figure 5), similar to the observation of Tutty &

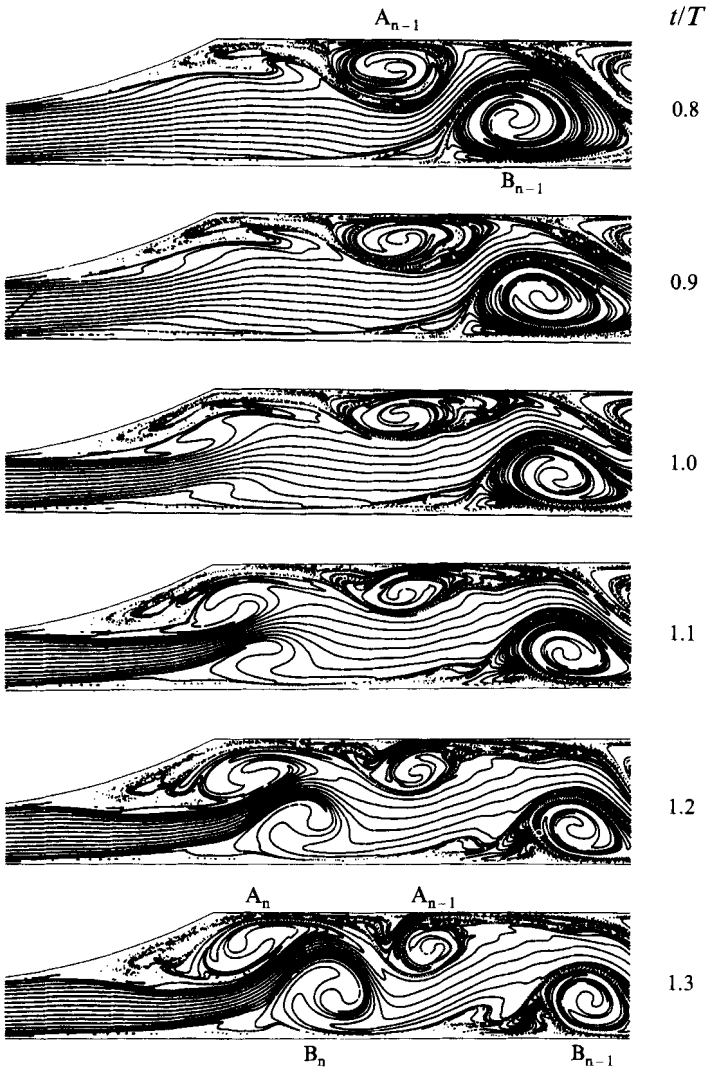

FIGURE 6. Streaklines in the formation region of the vortices ($Re = 360$, $St = 0.368$).

Pedley (1993), and no vorticity is entrained into the vortices from other sources during the formation phase. Consequently, the strength of the forming vortices is mainly determined by the properties of the boundary layers in the throat of the constriction.

3.4. *Propagation of the vortices*

Downstream of the formation region ($x > 13$), the flow field is dominated by the propagating vortices. The propagation (phase) speed of the vortices varies with the bulk flow: it is relatively small during the first half of the cycle and increases in the second half, along with the increase in the incoming velocity. The average propagation speed depends mainly on the mean velocity of the incoming flow (U_m) and is less dependent on the other parameters of the waveform. This conjecture was confirmed by a series of additional (unreported) simulations using different magnitudes of U_s and U_p (keeping the mean velocity U_m unchanged), as well as for other similar waveforms.

The steady incoming flow case was solved for a range of Reynolds numbers up to 3000. A steady flow is obtained as long as $Re < 1500$; for $Re > 1500$ the upper-wall shear layer becomes unstable, the eddy A breaks down and is periodically shed downstream. If the incoming flow is pulsating, moving vortices are generated even for Reynolds numbers as small as 90 (see §4), indicating that the forced time variation has a prominent effect on the formation mechanism. Indeed, the deceleration phase is responsible for amplifying the lateral velocity that carries vorticity into the core flow, see also Sobey (1982) and Ralph (1986).

To obtain two staggered trains of vortices at low Reynolds numbers (i.e. stable flows), the deceleration of the flow should take place in a non-symmetric channel. In a symmetric channel, symmetric vortices are generated unless the flow becomes unstable and the symmetry breaks down, in agreement with Sobey (1985) who pointed out that the dominating mechanism in the latter case is the instability of shear layers. In the present study, only stable flows are considered and trains of moving vortices develop because of the combination of pulsating incoming flow and asymmetric geometry.

Several previous studies found pulsating internal flow fields with a wavy core flow, see for example Pedley & Stephanoff (1985), Sobey (1985), Ralph & Pedley (1988, 1989) and Tutty & Pedley (1993). The wavy core flow is usually referred to as a 'vortex wave'. Vortex waves were discovered by Pedley & Stephanoff (1985) for the flow in a channel with an oscillating indentation. They developed a weakly nonlinear inviscid theory that related the generation of the vortex waves to the displacement of the vorticity gradient in the incoming Poiseuille flow. The term vortex wave has since been used to describe flows that are visually similar, even if the underlying mechanisms are different, Tutty & Pedley (1993).

4. Dependence on Reynolds number

The dependence of the flow field on the Reynolds number ($1500 > Re > 45$) was studied for a constant Strouhal number of 0.368. Figure 7 shows the instantaneous streamlines and vorticity field at $t/T = 0.2$ for several Reynolds numbers. The case with $Re = 45$ is not shown because propagating vortices were not found, although two stationary eddies (A_n and B_n) did form. Even for Re as low as 90 the eddies A_n and B_n propagate downstream (as was revealed in the time-sequence plots). Yet, at this low Re the vortices decay rapidly owing to enhanced viscosity and A_{n-1} and B_{n-1} survive for only a short portion of the cycle. In the case of $Re = 180$, two coexisting pairs can be observed during the entire cycle. The vortices get stronger and survive for a larger number of cycles as the Reynolds number increases, along with reduced damping of the transverse oscillations. Even at the highest Reynolds number shown ($Re = 1440$), instabilities are not detected and the deterministic events leading to the formation of A_n and B_n are similar to the low Reynolds number cases.

The formation region of the vortices moves upstream with the increase in the Reynolds number. The larger vorticity generated on the walls and the smaller retarding effects of the viscosity allow the roll-up to take place closer to the wall and at a more upstream section. The stronger vorticity generated near the walls is also responsible for the intensification of the vortices as the Reynolds number increases. Yet, time-sequence plots (not shown) reveal that the roll-up time is independent of the Reynolds number. This should not be surprising, because the vortex formation is dominated by the time variation of the forcing flow (through the increase of the lateral velocity in the deceleration phase). The waveform of the incoming velocity has not been changed and therefore the timing of the flow events should not vary significantly.

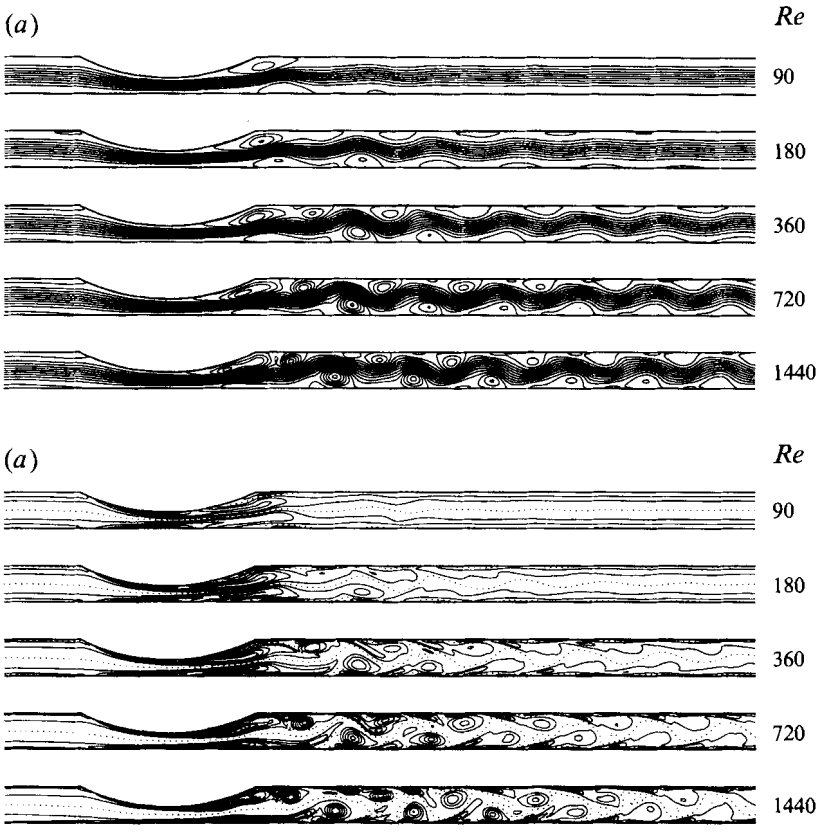

FIGURE 7. Dependence on Re ($t/T = 0.2$, $St = 0.368$): (a) the instantaneous streamlines and (b) the vorticity field. The increment between the vorticity contour lines is 5. Zero values are shown by dotted lines.

Figure 8 plots the axial location (x_v) of the B-vortex centre as a function of the Reynolds number. The location of the vortex centre was estimated from the time-sequence plots of the vorticity field (such as figure 5). The vortex B is followed in time as it moves downstream, rather than distinguishing between the vortices according to the cycle of formation. Three full cycles are shown, starting from $t/T = 0$ up to $t/T = 3$.

The axial position of the vortex centre at a given instance is shifted upstream as the Reynolds number increases, as was previously noted. However, the propagation speed (the slope of the lines) is independent of Reynolds number. Moreover, the variations in the propagation speed closely follow the variations of the incoming flow. In the steady flow phase, the propagation speed is constant, while during the acceleration and deceleration of the flow, it varies in phase with the incoming flow velocity. The Fourier decomposition of the axial velocity component revealed that the phase angles of the harmonics are locked to the incoming flow for all the Re tested, resulting in the direct relationship between the driving flow and the propagation speed of the vortices.

Figure 8 also presents the experimental results of Park (1989) for a similar geometry and St but $Re = 180$ (using our normalizations). The agreement in the location of B_n is very good. The agreement in B_{n-1} is less favourable, although still satisfactory con-

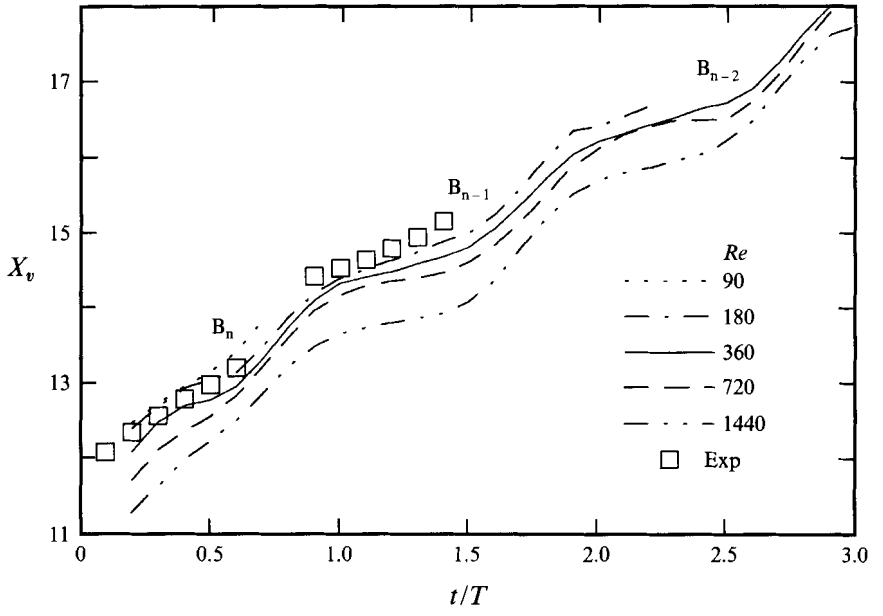

FIGURE 8. The dependence of the B-vortex centre location on the Reynolds number (St = 0.368), including experimental results of Park (1989).

sidering the difficulties in extracting the centre of diffused vortices from experimental visualizations.

5. Dependence on Strouhal number

The effect of Strouhal number ($12 > St > 0.01$) was studied for a constant Reynolds number of $Re = 360$ by changing the frequency of the incoming flow. The pattern of the flow field was found to be more sensitive to the Strouhal number than to the Reynolds number. Five different regimes with distinct flow properties were identified according to the Strouhal number: (i) very low-St regime ($0.02 > St$), (ii) low-St regime ($0.1 > St > 0.02$), (iii) intermediate-St regime ($0.75 > St > 0.1$), (iv) high-St regime ($2 > St > 0.75$) and (v) very high-St regime ($St > 2$).

The dependence of the vorticity field on St is given in figure 9 for $t/T = 0.2$ ($St = 0$ is the equivalent steady flow). For very low St ($St < 0.02$), the flow is approximately quasi-steady in the sense that the mean flow is identical to the equivalent steady flow. In the second half of the cycle the flow varies with time, while in the first half it is essentially steady. An elongated stationary eddy is found to the lee of the constriction during the whole cycle, but a B eddy is generated only in the second half of the cycle (and thus it cannot be observed in figure 9). A wavy core flow is formed only for a short time ($1 > t/T > 0.9$), when two additional eddies are generated downstream. The weak deceleration rate does not produce strong enough lateral velocity to carry substantial vorticity into the core, preventing the generation of vortices (although eddies with reversed flow do exist).

In the low-St regime ($0.1 > St > 0.02$), the stronger deceleration rate leads to the creation of well-defined vortices with a wavy core flow in the entire cycle. In the smallest St shown in this regime ($St = 0.023$), several elongated eddies are generated in the deceleration phase. Weak vortices develop at the downstream end of the eddies, but no roll-up of shear layers is observed. The situation is very different for $St = 0.046$

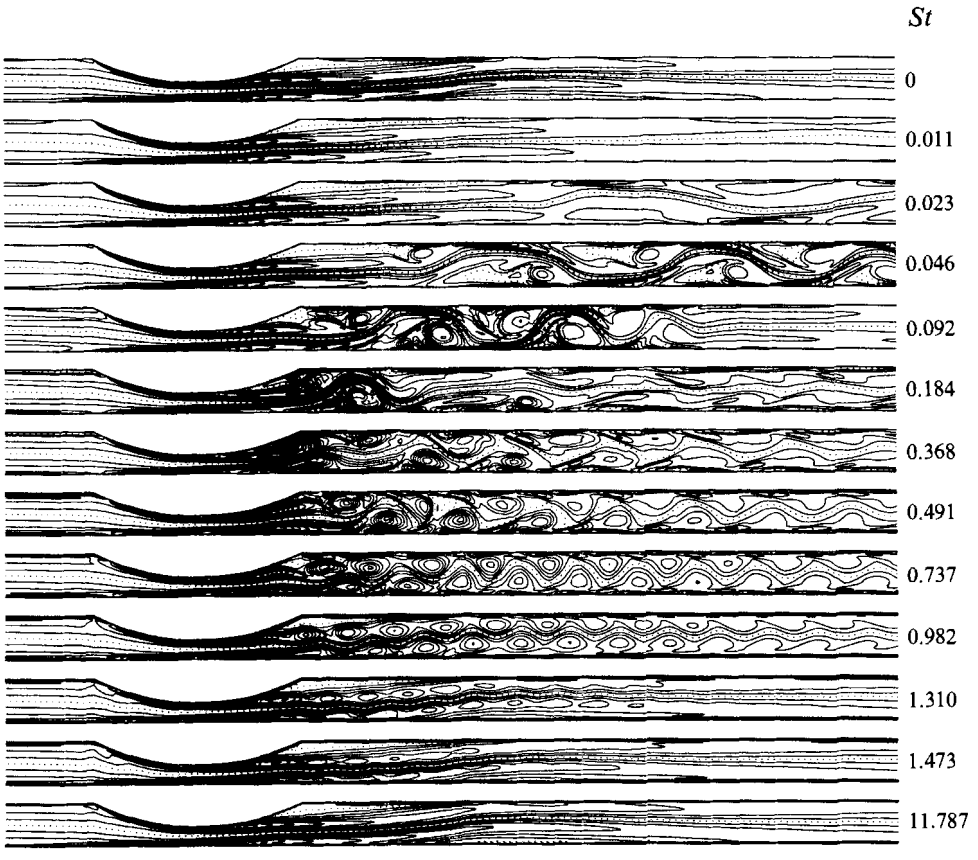

FIGURE 9. Dependence of the vorticity field on St ($t/T = 0.2$, $Re = 360$). Note that a particular phase of the cycle corresponds to a different absolute time for each St, because of the different period. The increment between the vorticity contour lines is 2.5. Zero values are shown by dotted lines.

and 0.092. In these cases, several shorter eddies develop and a vigorous wavy flow dominates the core for most of the cycle. Several vortices are generated in each cycle, in contrast to the base case, where only one pair of vortices is created per cycle (§3.3). The number of vortices decreases with the increase in St. Strong vortices develop at the downstream end of the eddies through the roll-up of shear layers originating from the upstream boundary layer. Secondary vortices may grow at the upstream part of the eddies (§6.2).

The intermediate-St regime ($0.75 > St > 0.1$) includes the base case ($St = 0.368$) that has already been described in detail (§3). At the low end of the regime ($St = 0.184$), only two pairs of vortices are created in each cycle. Vortices generated in the previous cycle can still be noticed downstream (although they are significantly weaker). For $St > 0.25$, only one pair of vortices is created in each cycle, while vortices generated in previous cycles are found downstream. The two trains of vortices, one near each wall, and the wavy core flow are characteristic to this regime. As St further increases, the vortices get stronger and shorter in length, the wavelength of the core flow decreases and the lateral oscillations are more vigorous. Although only one pair of vortices is created in each cycle, several cycles pass before the vortices fully develop at the high end of the regime ($St = 0.737$).

In the high-St regime ($2 > St > 0.75$), the flow field is distinguished by the diminishing vortices. The vorticity field in the core flow approaches that of the equivalent steady flow case modulated by the small-wavelength flow induced by the vortices. In the very high-St regime ($St > 2$), no vortices are created and the vorticity field is steady, except in very thin Stokes layers near the walls. In the core region the time derivative of the axial velocity is balanced by the pressure gradient; the convection and diffusion terms are negligible.

In the low-St regime, no thin boundary layer next to the wall develops, while in the intermediate-St regime such a layer is observed. In the first half of the cycle it consists of reversed flow regions beneath the vortices due to the high velocity enforced near the wall by the swirling motion of the vortices. In most of the second half of the cycle, the boundary layer flow is dominated by the large vorticity generated during the acceleration of the flow. In low-St cases, the period is long enough to diffuse away the excess vorticity without generating thin boundary layers. In the intermediate-St regime, on the other hand, the vorticity stays bound to the walls (except the vorticity in the shear layer emanating from the lee of the constriction) because of the shorter acceleration time. In the deceleration phase, a significant portion of the wall vorticity is advected into the core flow by the swirling motion of the vortices, §6.2. As the Strouhal number further increases, the vortices decrease in size and move away from the walls, allowing the establishment of thin Stokes layers along the whole length of the walls.

Previous works were mostly limited to the very small or small-St regimes, see table 1. In these regimes Tutty (1992) and Tutty & Pedley (1993), for example, found that as St increases the core flow responds more vigorously, the strength of the vortices increases and the wavelength depends mainly on St. Our simulations, which are consistent with these findings, extend the results to a wider St (and Re) regime.

Tutty (1992) and Tutty & Pedley (1993) used the streamfunction/vorticity formulation and finite difference discretization for solving the unsteady Navier–Stokes equations for cases with small St, while in the present work we employ a significantly different numerical scheme based on primitive variables and finite volume discretization. The agreement between the works in the global features of the flow field serves as an additional check on the validity of the numerical simulations. This validation of the numerical results is of special importance in the present case, where complementary experimental results do not exist.

6. Discussion

Several aspects of the vortical flow behind the constricted channel are elaborated in the present section. Special emphasis is given to describing the formation of the primary vortices for the various St regimes as well as to the secondary effects that locally modify the flow field.

6.1. *The properties and the development of the vortical flow field*

The characteristics of the flow field were found to depend on the Strouhal number. Yet, the formation of vortices and their propagation downstream is common to all St, except for the two extremes of very high and very low St. The vortex formation mechanism in the low-St regime is identical to that described by Tutty & Pedley (1993) for the case of an oscillating flow behind a stepped channel. Hence, it will be only briefly reviewed here for the completeness of the description. The main emphasis will be on the influence of St on the flow field behind the constriction.

The vortex A in the lee of the constriction is quasi-stationary; it exists during the whole cycle at any St and the role of the oscillations in the creation of A is minor. It is generated even in low Reynolds number flows with steady incoming velocity. In the deceleration phase ($1 > t/T > 0.75$) of the low-St regime, large lateral flow develops near the lower wall. Vorticity is carried away from the wall into the core, forming by $t/T = 0.7$ an eddy farther downstream on the lower wall (as was seen in a detailed examination of the sequence of streamlines and vorticity field for the $St = 0.046$ case). The displacement of the streamlines downstream of the lower-wall eddy and the deceleration of the flow enhance the convection of vorticity from the upper wall into the core, forming a third eddy ($t/T = 0.8$), that in turn induces yet another eddy near the lower wall farther downstream ($t/T = 0.9$). This process of successive eddy generation continues in the steady incoming flow phase, forming a total of four pairs of vortices by $t/T = 1.2$ ($= 0.2$) (only three pairs can be observed in the domain shown). The downstream parts of the eddies roll up into relatively strong vortices, while in the upstream part a secondary vortex grows in the steady incoming phase (§6.2). The vortices are washed away in the second half of the cycle, with the increase in the mass flow rate.

The vortex formation mechanism in the low-St regime is identical to that described by Tutty & Pedley (1993), although the two cases differ in many details, including in the geometry of the constriction and in the waveform of the forcing flow. This indicates that the oscillation of the incoming flow is a major factor in the establishment of the vortical flow (together with the non-uniform channel). Supporting evidence can be found in the analysis of very small-St flows. In the latter case, as well as in steady flows, a wavy core flow does not develop for $Re < 1500$. Two essentially stationary eddies form – one long eddy in the lee of the constriction and another small eddy on the lower wall, figures 3 and 9. Although shear layers emanate from the throat of the constriction, similar to the higher-St cases, they do not roll up and do not form vortices. Continuous forced oscillations (of sufficient strength) seem to be necessary for the generation of multiple vortices in stable flows.

The mean flow, on the other hand, does not generate vortices but plays a passive role of advecting them downstream. In our opinion, in the cases considered by Tutty & Pedley (1993) and Sobey (1982, 1985), the vortices were essentially stationary because the mean flow is zero. In the present case, as well as in Pedley & Stephanoff (1985), Ralph & Pedley (1988, 1989) and Tutty (1992), propagating vortices are found because the non-vanishing mean of the flow forces the whole system of vortices to move.

The number of successive vortices created in each cycle depends on the period. As Strouhal increases (shorter period) less time remains for the repetition of the vortex generation mechanism and fewer vortices form downstream in the same cycle. For $St = 0.092$, for example, three pairs of vortices are generated while for $St = 0.046$ four pairs of vortices were found. The vortex generation mechanism proposed by Tutty & Pedley (1993) predicts a phase lag in the development and roll-up of the successive vortices because of the convective mechanism. The more downstream a vortex is, the later in the cycle it is created, it is less developed and the wavelength of the core flow decreases. All these predictions for low St were found to hold true in the present simulations as well.

In the intermediate-St regime, the stronger deceleration rate causes the roll-up of A_n closer to the constriction and the subsequent creation of B_n a small distance downstream by the same mechanism as that in the low-St regime. The difference between the roll-up time of A_n and B_n is small, so that they seem to be created

simultaneously. The vortices are almost circular in shape, in contrast to the small-St regime that was characterized by elongated eddies. The shorter period does not leave enough time to create additional vortices in the same cycle for $St > 0.25$. In the acceleration phase the vortices are carried downstream, but because of the shorter time involved they are not washed away from the region shown. Thus, at every instant several pairs of vortices can be observed. Each pair is created in a different cycle, rather than in the same cycle as in the low-St regime. This is a major difference with previous studies, except that of Park (1989). Most existing studies considered low-St flows and therefore the multiple vortices were all created in the same cycle.

In the high-St regime the size of the vortices decreases with St because A_n does not have enough time to fully form before it is carried away and another vortex is formed in the next cycle. The smaller A_n induces an even weaker B_n vortex. Also, the shear layer emanating from the constriction rolls up at a shorter distance from the constriction as St increases. In the intermediate-St regime, B_n had its maximal strength and size immediately after it was formed, while for high St, B_n continues to grow in the next few cycles. In the case of $St = 0.982$, for example, approximately four cycles are required until B fully forms (figure 9). As St increases even more, vortices do not form because the flow field cannot accommodate to the rapid changes in the forcing flow, inhibiting the roll-up of shear layers. For $St \gg 1$, the vorticity field in the core is steady because $St\,\partial\omega/\partial t \gg -\boldsymbol{u}\cdot\nabla\omega + 1/Re\nabla^2\omega$ (ω is the vorticity) and thus $\partial\omega/\partial t \approx 0$.

For all Strouhal numbers, except near the two ends of the regime, a wavy core flow is found. For $St < 0.15$ the wavy core flow is recreated in each cycle by the successive vortex generation mechanism without residual vortices from the previous cycle, Tutty & Pedley (1993). The wavefront (group) velocity is larger than the propagation (phase) velocity of the vortices and the wavelength decreases in the downstream direction. For $St > 0.25$ only one pair of vortices is generated in each cycle and consequently the wavelength is equal to the distance between the adjacent vortices. Contrary to small Strouhal number flows, the wavelength does not vary in the downstream direction.

The generation of vortices and the development of the core flow are strongly coupled in the low-St regime owing to the successive vortex generation mechanism. In the intermediate- and high-St regimes, however, this mechanism acts for the creation of the first pair of vortices only. From then on, the propagation of the vortices dominates the flow field and creates the wavy core flow. This is yet another major difference with most other numerical and theoretical studies.

The number of vortex pairs and hence the wavelength, depends on St in all the regimes. Increasing St decreases the wavelength, similar to the finding of Tutty & Pedley (1993) for low St. For intermediate and high St, the number of coexisting vortices increases with St, while for low St the number of vortices decreases with St. Thus, there is a local minimum in the number of coexisting vortices. In the present study, the minimum is found at $St \approx 0.18$, figure 9.

Although viscosity is responsible for generating vorticity, the role of viscosity is less important than the role of vortex dynamics in determining the global vortical flow pattern. Convection is responsible for carrying vorticity into the core flow through concentrated shear layers and their subsequent roll-up into vortices. Global features, such as the wavelength, propagation speed and the interactions between the primary vortices are essentially inviscid. This is especially true for intermediate St, where the flow is dominated by the propagating vortices. The viscosity, however, determines the strength of the shear layers and consequently the strength of the vortices. It also

affects the location of the formation region and to some extent secondary effects such as vorticity cancellation (§6.2).

Propagating wave trains can be also created by inviscid perturbations, as was found for the case of an oscillating indentation (Pedley & Stephanoff 1985; Ralph & Pedley 1988, 1989) or for a rigid expanding channel with an oscillating incoming flow, (Tutty & Pedley 1994). These waves can be viewed as the inviscid limit of Tollmien-Schlichting waves generated deterministically, (Tutty & Pedley 1994). This inviscid wave generation mechanism is dominant in low-St cases with small constriction sizes, where concentrated shear layers do not develop. However, for high St as well as for cases where strong shear layers are generated (as in the present case as a result of the large constriction size), the theory of Tutty & Pedley (1994) cannot be expected to yield an accurate description of the flow field. Strong nonlinear vortex dynamics governs the flow field in this case, see also Tutty & Pedley (1993).

6.2. *Secondary effects*

The generation of the primary system of vortices was elaborated in the previous section. The non-uniform geometry and the pulsating forcing flow were found to play the major role in the establishment of the vortical flow behind the constriction. This vortex system might be further modified in certain regimes of St and Re by secondary effects. Three secondary effects are discussed here: the evolution of secondary vortices upstream of the primary vortices, vorticity cancellation that reduces the strength of the vortices and the opposite mechanism of vorticity feeding that strengthen the vortices. In contrast to the primary flow phenomena, the secondary effects are local processes. The incoming waveform or the constriction size are less dominant in their evolution than local flow structures.

The first phenomenon of the evolution of secondary vortices was described by Tutty & Pedley (1993) for low-St cases. The long period of small Strouhal flows not only allows the generation of several primary vortices in each cycle, but also leads to the development of secondary vortices, see for example figure 9 ($St = 0.046$) and figure 10. The latter figure zooms in to the region of the most upstream primary B eddy for the case of $St = 0.046$ at $t/T = 0$. The secondary vortex in the upstream part of each primary vortex is created by the roll-up of two shear layers, figure 10. One shear layer originates from the wall upstream of the vortex (the same shear layer generated the main vortex as well). The second shear layer is pulled from the core by the swirling motion of the contra-rotating eddy D created near the wall by the primary vortex (figure 10). The secondary vortex rolls up by $t/T = 0.2$ (figure 9), but exists for only a short time (by $t/T = 0.3$ it disappears). The creation of secondary vortices is limited to the low-St regime. As St increases, less time remains for the completion of the roll-up of the secondary vortex before all the vortices are washed away. For $St > 0.2$, secondary vortices are not formed at all.

The larger mass flow rate inhibits the vortices from growing to the full height of the channel, in contrast to the findings of Tutty & Pedley (1993). In the latter case, the secondary vortex was generated during the deceleration, close to the instant of vanishing mass flow rate. In the present case, the same mechanism acts during the steady incoming flow phase, indicating that local vortex dynamics is responsible for the generation of the secondary vortex, rather than the time variation of the driving flow.

The rotational motion of the vortices drags counter-vorticity from the wall beneath the upstream part of the vortices into the core flow, see for example vortex D in figure 10. The counter-vorticity augments vorticity cancellation and thus the self-

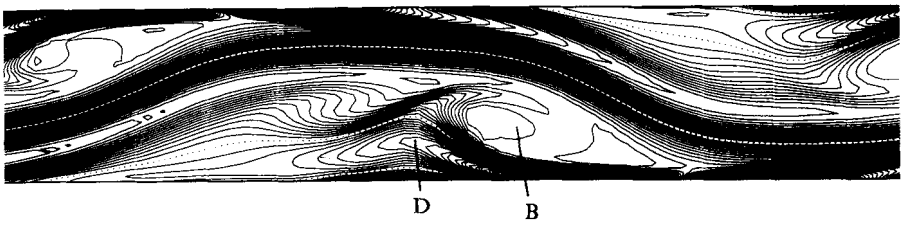

FIGURE 10. The development of the secondary vortex ($t/T = 0$, $Re = 360$, $St = 0.046$). The increment between the vorticity contour lines is 1. Zero values are shown by dotted lines.

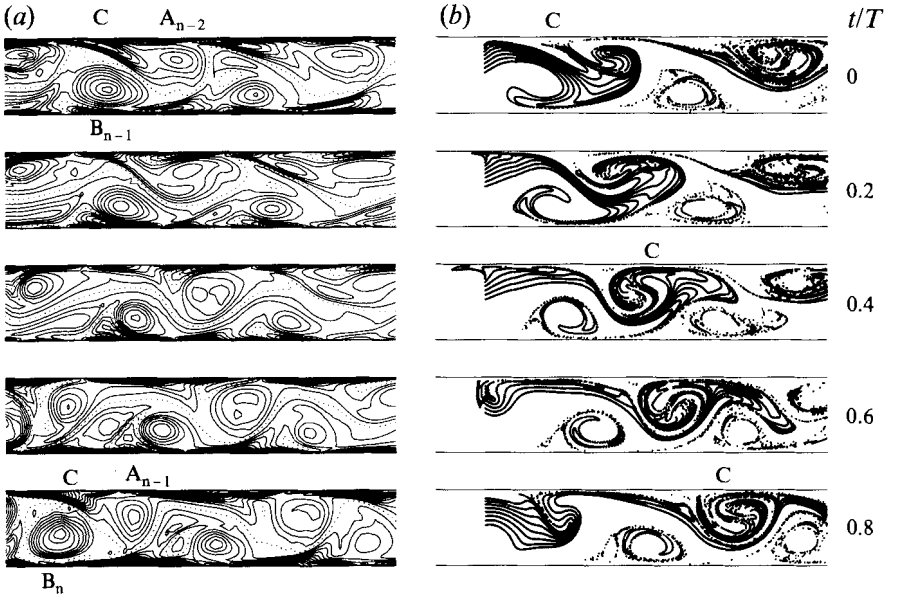

FIGURE 11. Feeding of vorticity ($Re = 360$, $St = 0.368$): (*a*) vorticity field, (*b*) streaklines. The increment between the vorticity contour lines is 2.5. Zero values are shown by dotted lines.

destruction of the vortices. Significant vorticity cancellation is observed in the low- and especially intermediate-St regimes because the vortices are strong enough to extract significant counter-vorticity from the wall. In the high-St regime, the vortices are not only weaker, but are displaced away from the walls and therefore vorticity cancellation is negligible.

In the intermediate-St regime, the secondary effects may modify the vortical flow in the propagation region. The decay of the vortices by vorticity cancellation might be counterbalanced by vortex strengthening through the feeding of same-sign vorticity from the wall into existing vortices. The relatively strong swirling motion of B_n in the intermediate-St regime and its $O(1)$ size pull a shear layer of counter-vorticity from the upper wall as well, upstream of A_{n-1}, see figures 5 and 11. Figure 11 gives for the base case the vorticity field and the streaklines in the region $18 > x > 13$ of the channel (the downstream edge of the constriction is at $x = 11.7$). The streaklines are released from several points near the upstream wall only to concentrate on the flow structures of interest.

The shear layer C produced by B starts to develop in the acceleration phase of the cycle, when large amount of vorticity is generated on the walls. It extends away from

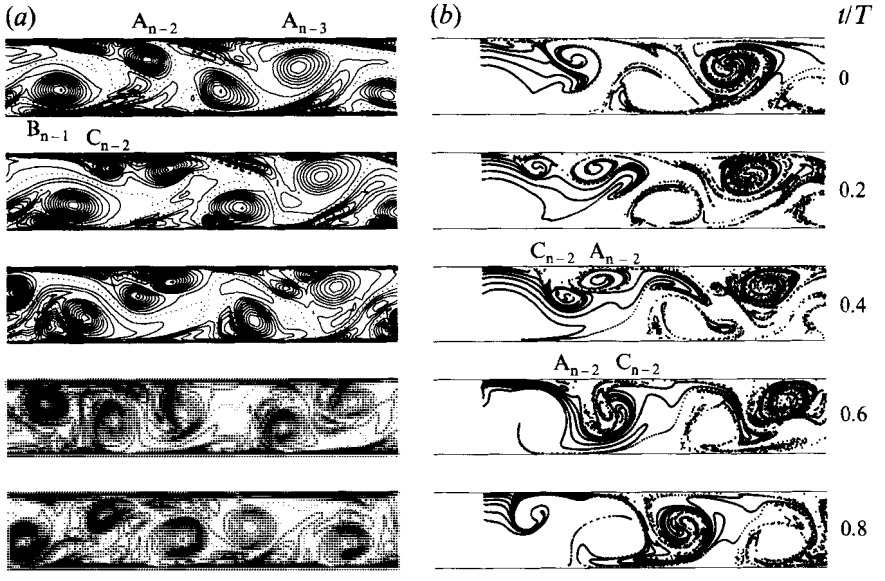

FIGURE 12. Feeding of vorticity with vortex coalescence ($Re = 1440$, $St = 0.368$): (*a*) vorticity, (*b*) streaklines. The increment between the contour lines is 2.5. Zero values are shown by dotted lines.

the wall during the deceleration phase (see $t/T = 0.8$). In the initial phase of the steady incoming velocity it reaches the core flow and by $t/T = 0.2$ it is entrained into the core of A_{n-2} (the indices of the vortices are shifted by 1 because the next cycle has started). The vorticity originating from the shear layer C keeps its separate identity in the vortex core until the end of the cycle, generating separate closed vorticity contour lines in the core of A_{n-2}. However, the streaklines reveal that the vortex has only one core. The vorticity included in the shear layer has the same sign as that of A_{n-2} and therefore the feeding of vorticity increases the overall strength of A_{n-2}, as is clearly observed in the later phases of the cycle (figures 5 and 11). Vortex feeding (though of reduced strength) is found for the farther downstream A vortices, as well as for the B vortices.

Viscosity has a more pronounced influence on the local secondary effects than on the global flow structures. Consequently, the details of vorticity feeding depend on the Reynolds number. As the Reynolds number increases, stronger shear layers develop and they may roll up before they are captured by the core of existing vortices. Such a case is shown in figure 12 which presents the vorticity field and the streaklines for $Re = 1440$ and $St = 0.368$ ($18 > x > 13$). By $t/T = 0$, a shear layer is created upstream of A_{n-2}, as in the lower-Re case. However, this shear layer is significantly stronger and by $t/T = 0.2$ it rolls up into a separate vortex C_{n-2}. C_{n-2} expands and moves away from the wall, while accelerating its downstream speed. By $t/T = 0.4$, C_{n-2} catches up with A_{n-2} and the two vortices roll one around the other, maintaining their distinct cores and gradually coalescing into a single core vortex (A_{n-3}) by $t/T = 1.4$ (i.e. in the next cycle). In this case as well, the net effect is the augmentation of the A vortices, although the mechanism is more complex than the direct feeding mechanism found for the lower-Re cases.

Both vorticity cancellation and vortex feeding are a result of the interaction between existing vortices and the walls. While vorticity cancellation can be obtained in external

flows as well (Doligalski & Walker 1984), vortex feeding by the present mechanism is possible only in internal flows, provided the size of the vortices is of the same order as the height of the channel.

In the high-St regime, the structure of the vortical flow behind the constriction is considerably simpler because the secondary effects are negligible, figure 9. Moreover, the vortices do not interact with each other or with the walls because of the short period. Consequently, the vortices propagate downstream almost intact, apart from the changes in size due to the continuation of the roll-up process in the next few cycles. Their strengths decay slowly due to diffusion, but are almost unaffected by vorticity cancellation or by feeding of vorticity.

REFERENCES

ARMALY, B. F., DURST, F. J. PEREIRA, C. F. & SCHONUNG, B. 1983 Experimental and theoretical investigation of backward-facing step flow. *J. Fluid Mech.* **127**, 473–496.

DOLIGALSKI, T. L. & WALKER, J. D. A. 1984 The boundary layer induced by a convected two-dimensional vortex. *J. Fluid Mech.* **139**, 1–28.

PARK, D. K. 1989 A biofluid mechanics study of arterial stenoses. MSc thesis, Lehigh University, Bethlehem, Pennsylvania.

PEDLEY, T. J. & STEPHANOFF, K. D. 1985 Flow along a channel with a time-dependent indentation in one wall: the generation of vorticity waves. *J. Fluid Mech.* **160**, 337–367.

RALPH, M. E. 1986 Oscillatory flows in wavy-walled tubes. *J. Fluid Mech.* **168**, 515–540.

RALPH, M. E. & PEDLEY, T. J. 1988 Flow in a channel with a moving indentation. *J. Fluid Mech.* **190**, 87–112.

RALPH, M. E. & PEDLEY, T. J. 1989 Viscous and inviscid flows in a channel with a moving indentation. *J. Fluid Mech.* **209**, 543–566.

ROSENFELD, M. 1993 Validation of numerical simulation of incompressible pulsatile flow in a constricted channel. *Computers & Fluids* **22**, 139–156.

ROSENFELD, M. & KWAK, D. 1991 Time-dependent solutions of viscous incompressible flows in moving coordinates. *Intl J. Numer. Meth. Fluids* **13**, 1311–1328.

ROSENFELD, M. & KWAK, D. 1993 Multi-grid acceleration of fractional step solvers of incompressible Navier-Stokes equations in generalized curvilinear coordinate systems. *AIAA J.* **31**, 1792–1800.

ROSENFELD, M., KWAK, D. & VINOKUR, M. 1991 A fractional-step solution method for the unsteady incompressible Navier-Stokes equations in generalized coordinate systems. *J. Comput. Phys.* **94**, 102–137.

SOBEY, I. J. 1982 Oscillatory flows at intermediate Strouhal number in asymmetric channels. *J. Fluid Mech.* **125**, 359–373.

SOBEY, I. J. 1985 Observation of waves during oscillatory channel flow. *J. Fluid Mech.* **151**, 395–426.

TUTTY, O. R. 1992 Pulsatile flow in a constricted channel. *J. Biomech. Engng* **114**, 50–54.

TUTTY, O. R. & PEDLEY T. J. 1993 Oscillatory flow in a stepped channel *J. Fluid Mech.* **247**, 179–204.

TUTTY, O. R. & PEDLEY T. J. 1994 Unsteady flow in a nonuniform channel: A model for wave generation. *Phys. Fluids* A **6**, 199–208.